Available online at www.sciencedirect.com
SCIENCE DIRECT®
Composites: Part B 35 (2004) 551–556
composites Part B: engineering
www.elsevier.com/locate/compositesb

# Fracture analysis of facesheets in sandwich composites

H. Jiang[a], Y. Huang[a,*], C. Liu[b]

[a]Department of Mechanical and Industrial Engineering, University of Illinois, 1206 West Green Street, Urbana, IL 61801, USA
[b]MST-8, Los Alamos National Laboratory, Los Alamos, New Mexico 87545, USA

Received 6 June 2003; accepted 11 January 2004
Available online 21 July 2004

**Abstract**

There exist two fracture mechanisms in facesheets of sandwich composites consisting of the 0° and 90° plies, namely crack growth and crack blocking. The former is undesired since it may lead to failure of facesheets and even the core in sandwich composites. A shear-lag model is developed in this article and it gives a simple criterion governing these two mechanisms. It is established that, for a given ratio $E_t/E_f$ of the elastic moduli in the transverse and fiber directions, there exists a critical facesheet thickness above which crack blocking is achieved and crack growth is prevented.


*Keywords:* A. Fibres; A. Lamina/ply; B. Fracture; Shear-lag

## 1. Introduction

Because of their high modulus/weight and strength/weight ratios, composites have many important applications in naval structures [1,2], as well as in automotive, aerospace, and other defense industries. For example, carbon/carbon laminated composites have been used as the leading panels on the space shuttle wing, and used as the outer shell of other re-entry vehicles. The primary function of the carbon/carbon composites is acting as the thermal shield. Due to the uneven distribution of temperature, the carbon/carbon composite will be subjected to substantially high level of internal stress. Under such high stress, if any of the defect on the outer surface propagates through the composite thermal shield, it will lead to disastrous consequences as exemplified by the recent accident of the space shuttle Columbia. To ensure the composite sheet to have sufficient strength so that a crack cannot go through it to reach the inner structure, thus becomes a paramount concern in composite design.

Sandwich composites consist of the core material sandwiched by facesheets and the facesheets are made of laminated composites. Fig. 1a shows a schematic diagram of a facesheet made of alternating 0° and 90° plies, though some facesheets have other microstructures (e.g. ±45° plies, woven composites). The thickness of each ply is $t$, while the thickness of facesheet is $b = N_{total}t$, where $N_{total}$ is the total number of plies. Let $x_1$ denote the normal direction of the plies, and $x_2$ and $x_3$ represent the fiber directions (i.e. directions of reinforcement) in the 0° and 90° plies, respectively.

The purpose of this article is to study fracture of facesheets in sandwich composites, and to establish a simple design criterion for facesheets against fracture. Fig. 1b shows the schematic diagram of the facesheet that has a pre-crack of size $a$ along the $x_1$ direction, where $a = N_{crack}t$, and $N_{crack}$ is the number of broken plies prior to loading. The pre-crack is arrested by an intact 0° ply (Fig. 1b). Since the 0° plies have fibers normal to the crack plane, they remain intact during loading and provide resistance to crack growth. On the contrary, fibers in the 90° plies are parallel to the crack plane and cannot resist crack growth. Here crack growth takes the form of microcrack nucleation across the 90° plies upon loading.

As the load is applied to the facesheet, the first microcrack is always nucleated on the crack plane in the first 90° ply closest to the pre-crack (Fig. 1c) because of the stress concentration due to the pre-crack. One important question is that, as the applied load increases, will microcracks be nucleated in the subsequent 90° plies as shown schematically in Fig. 2a? Or alternatively, will the subsequent microcrack nucleation be confined in a small zone around the pre-crack tip, such as the idealized situation of subsequent microcracks confined within the first 90° ply

* Corresponding author. Tel.: +1-217-265-5072; fax: +1-217-244-6534.
*E-mail address:* huang9@uiuc.edu (Y. Huang).

1359-8368/$ - see front matter © 2004 Elsevier Ltd. All rights reserved.
doi:10.1016/j.compositesb.2004.01.005

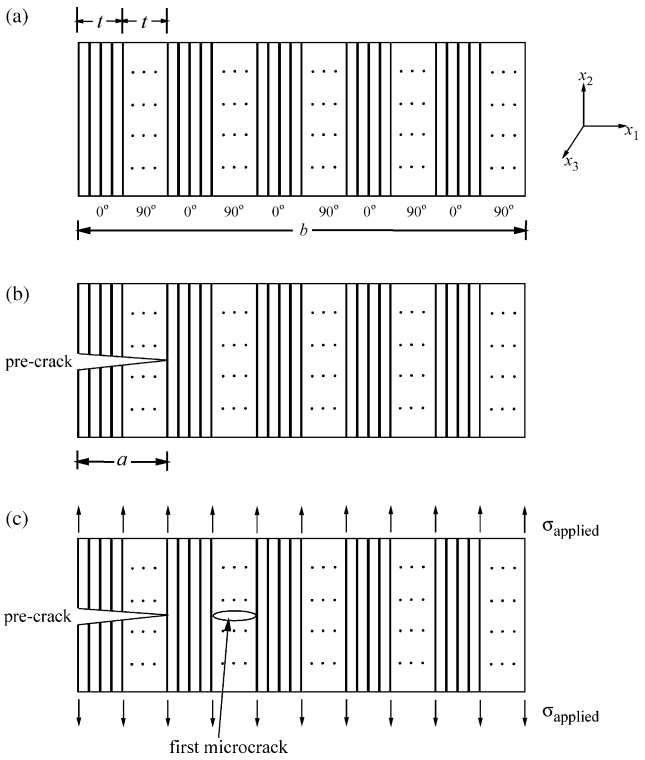


Fig. 1. (a) A schematic diagram of alternating 0° and 90° plies in a facesheet of sandwich composite; the ply thickness is $t$ and the facesheet thickness is $b$; $x_1$ denotes the normal direction of the plies, and $x_2$ and $x_3$ are along the fiber directions in the 0° and 90° plies, respectively. (b) A schematic diagram of the alternating 0° and 90° plies in a facesheet with a pre-crack of length $a$. (c) A schematic diagram for first microcrack nucleation in the 90° ply next to the pre-crack tip.

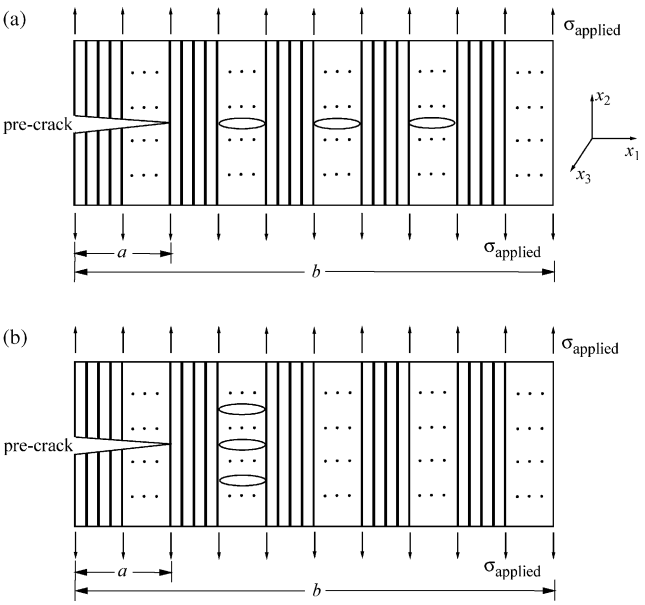


Fig. 2. (a) Crack growth mechanism through microcrack nucleation across the 90° lies in a facesheet with alternating 0° and 90° plies; the applied stress is $\sigma_{\text{applied}}$. (b) crack blocking mechanism via microcrack nucleation confined in the same 90° ply next to the pre-crack tip.

as shown schematically in Fig. 2b? The former will lead to the undesired crack propagation in the 90° plies across the facesheet. In other words, even though the 0° plies remain intact, the pre-crack effectively propagates through the facesheet. The latter (microcracks confined in the first 90° ply) will prevent crack propagation in the facesheet and therefore protect the sandwich composites. These two mechanisms shown in Figs. 2a and 2b are called crack growth and crack blocking, respectively.

The shear-lag model was developed more than half a century ago to study single or multiple stringer panels in aerospace structures [3]. It has been successfully applied to metal-ceramic laminates [4,5] and fiber-reinforced metal matrix composites [6]. We use the shear-lag model to study fracture of facesheets in sandwich composites. The shear-lag model is developed in Section 2 to examine the critical condition governing the crack growth and crack blocking mechanisms in facesheets. The results are presented in Section 3, and they lead to a very simple design criterion against fracture of facesheets.

## 2. Shear-lag model

### 2.1. Elastic moduli of the 0° and 90° plies

For simplicity, we assume that the facesheet is under plane-strain deformation, i.e. $\varepsilon_{33} = 0$ in each ply, though the analysis can be easily modified for plane-stress deformation if desired. Let $E_f$ and $E_t$ denoted the (plane-strain) elastic moduli in the fiber direction and in the transverse (normal to fiber) direction, respectively. They are the elastic moduli in the $x_2$ direction of the 0° and 90° plies. The shear moduli in the plane parallel and normal to fibers are denoted by $\mu_f$ and $\mu_t$, respectively, and they are the in-plane ($x_1 - x_2$) shear moduli of the 0° and 90° plies.

### 2.2. Governing equations in the shear-lag model

Fig. 3 shows a representative element of the $n^{\text{th}}$ ply in the shear-lag model, where $n = 1, 3, 5, \ldots$ for the 0° plies,

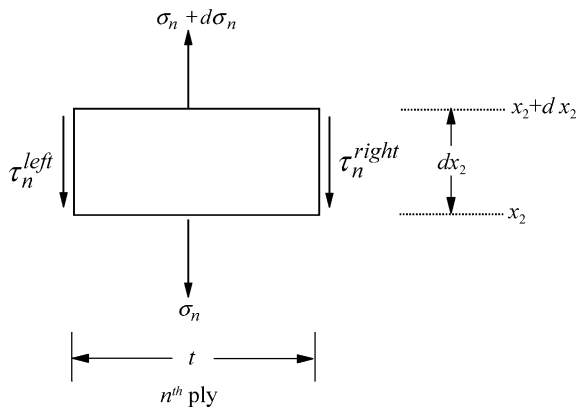


Fig. 3. An infinitesimal element of a ply in the shear-lag model.

and 2,4,6… for 90° plies (Figs. 1 and 2). For example, $n = 1$ is the leftmost 0° ply, $n = N_{\text{crack}} + 1$ is the first intact 0° ply after the pre-crack, $n = N_{\text{crack}} + 2$ is the 90° ply in which the first microcrack is nucleated, and $n = N_{\text{total}}$ is the last ply on the right. Here we have taken the leftmost ply to be a 0° ply (Figs. 1 and 2). The axial stress in each ply is averaged over the ply thickness $t$, and is denoted by $\sigma_n = \sigma_n(x_2)$ for the $n^{\text{th}}$ ply. The shear tractions at the interfaces with the left and right plies (n − 1 and $n + 1$) are denoted by $\tau_n^{\text{left}}$ and $\tau_n^{\text{right}}$, respectively, as shown in Fig. 3. For the representative element in Fig. 3, the equilibrium requires

$$t\frac{\mathrm{d}\sigma_n}{\mathrm{d}x_2} = \tau_n^{\text{left}} + \tau_n^{\text{right}}. \tag{1}$$

Let $w_n = w_n(x_2)$ denote the axial displacement at the center of the $n^{\text{th}}$ ply, and $w_n^{\text{left}}$ and $w_n^{\text{right}}$ be the axial displacement at the interfaces with the left and right plies ($n - 1$ and $n + 1$), respectively. The shear tractions in the $n^{\text{th}}$ layer are related to these displacements by

$$\tau_n^{\text{left}} = \mu_n \frac{w_n - w_n^{\text{left}}}{t/2}, \qquad \tau_n^{\text{right}} = \mu_n \frac{w_n - w_n^{\text{right}}}{t/2}, \tag{2}$$

where $\mu_n = \mu_f$ for the 0° plies ($n = 1, 3, 5, \ldots$), and $\mu_n = \mu_t$ for the 90° plies ($n = 2, 4, 6, \ldots$). The normal stress $\sigma_n$ in the $n^{\text{th}}$ ply is related to the displacement $w_n$ by

$$\sigma_n = E_n \frac{\mathrm{d}w_n}{\mathrm{d}x_2}, \tag{3}$$

where $E_n = E_f$ and $E_n = E_t$ for the 0° and 90° plies, respectively.

The equilibrium also requires the shear tractions to satisfy

$$\tau_n^{\text{left}} = -\tau_{n-1}^{\text{right}}, \qquad \tau_n^{\text{right}} = -\tau_{n+1}^{\text{left}}. \tag{4}$$

If there is no interface debonding, the continuity of displacements across the interface between plies requires

$$w_n^{\text{left}} = w_{n-1}^{\text{right}}, \qquad w_n^{\text{right}} = w_{n+1}^{\text{left}}. \tag{5}$$

We eliminate the displacement at the interfaces from Eqs. (2), (4), and (5), and obtain the shear tractions as

$$\tau_n^{\text{left}} = \frac{w_n - w_{n-1}}{\frac{t}{2}\left(\frac{1}{\mu_f} + \frac{1}{\mu_t}\right)}, \qquad \tau_n^{\text{right}} = \frac{w_n - w_{n+1}}{\frac{t}{2}\left(\frac{1}{\mu_f} + \frac{1}{\mu_t}\right)}. \tag{6}$$

Its substitution into the equilibrium Eq. (1) yields

$$\frac{t^2}{2}\left(\frac{1}{\mu_f} + \frac{1}{\mu_t}\right)\frac{\mathrm{d}\sigma_n}{\mathrm{d}x_2} = 2w_n - w_{n-1} - w_{n+1}. \tag{7}$$

Eqs. (3) and (7) give a set of ordinary differential equations for all plies except the leftmost ($n = 1$) and the last one to the right ($n = N_{\text{total}}$). For the leftmost ply ($n = 1$) which has traction-free condition $\tau_1^{\text{left}} = 0$, (7) becomes

$$\frac{t^2}{2}\left(\frac{1}{\mu_f} + \frac{1}{\mu_t}\right)\frac{\mathrm{d}\sigma_1}{\mathrm{d}x_2} = w_1 - w_2. \tag{8}$$

The last ply on the right ($n = N_{\text{total}}$) is attached to the core in sandwich composites. Its boundary condition is somewhat complex. Here we examine two limiting cases.

*(i) very compliant core material*

The interaction between the last ply and the core is weak such that it can be approximated by the traction-free condition $\tau_{N_{\text{total}}}^{\text{right}} = 0$ for a very compliant core. Eq. (7) then becomes

$$\frac{t^2}{2}\left(\frac{1}{\mu_f} + \frac{1}{\mu_t}\right)\frac{\mathrm{d}\sigma_{N_{\text{total}}}}{\mathrm{d}x_2} = w_{N_{\text{total}}} - w_{N_{\text{total}}-1}. \tag{9}$$

*(ii) very stiff core material*

The displacement at the interface between the last ply and the core is essentially zero, $w_{N_{\text{total}}}^{\text{right}} = 0$, for a very stiff core. The substitution of $\tau_{N_{\text{total}}}^{\text{left}}$ in (6) and $\tau_{N_{\text{total}}}^{\text{right}} = \mu_{N_{\text{total}}} \frac{w_{N_{\text{total}}}}{t/2}$ in Eq. (2) into the equilibrium Eq. (1) gives

$$\frac{t^2}{2}\left(\frac{1}{\mu_f} + \frac{1}{\mu_t}\right)\frac{\mathrm{d}\sigma_{N_{\text{total}}}}{\mathrm{d}x_2} = \left(1 + \frac{\mu_{N_{\text{total}}}}{\mu_f} + \frac{\mu_{N_{\text{total}}}}{\mu_t}\right) w_{N_{\text{total}}} - w_{N_{\text{total}}-1}, \tag{10}$$

where $\mu_{N_{\text{total}}} = \mu_f$ or $\mu_t$ if the last ply is the 0° ply or 90° ply, respectively.

Eqs. (7–9) or 10 constitutive the governing equations of the shear-lag model.

### 2.3. Boundary conditions

We focus on the configuration in Fig. 1c in which the first microcrack has been nucleated. The traction is free on the faces of the pre-crack and the first microcrack, i.e.

$$\sigma_n = 0 \qquad \text{at } x_2 = 0 \qquad \text{for } n \le N_{\text{crack}} \qquad \text{or} \qquad n = N_{\text{crack}} + 2. \tag{11}$$

For plies that remain intact, we have

$$w_n = 0 \qquad \text{at } x_2 = 0 \qquad \text{for } n = N_{\text{crack}} + 1 \qquad \text{or} \qquad n \ge N_{\text{crack}} + 3. \tag{12}$$

A uniform remote strain, $\varepsilon_{\text{applied}}$, is imposed to all plies, i.e.

$$\frac{\mathrm{d}w_n}{\mathrm{d}x_2} = \varepsilon_{\text{applied}} \qquad \text{as } x_2 \to +\infty \text{ for all } n. \tag{13}$$

The remote applied stress is then given by

$$\sigma_{\text{applied}} = \frac{1}{2}(E_f + E_t)\varepsilon_{\text{applied}}. \tag{14}$$

## 3. Design criterion against fracture of facesheets in sandwich composites

We use IMSL Program [7] to numerically solve governing equations and boundary conditions in Section 2.3. The numerical results presented in the following lead to a very

simple design criterion against fracture of facesheets in sandwich composites.

First of all, the numerical results have suggested that, unless the pre-crack is so long that it almost reaches the last ply on the right (i.e. $a \sim b$, or equivalently $N_{\text{crack}} \sim N_{\text{total}}$), the stress in plies near the pre-crack tip for very compliant core (i.e. Eq. (9)) is the same as that for very stiff core (i.e. Eq. (10)). Therefore, we present only results that are based on boundary condition (9) in the following.

### 3.1. Non-dimensional material parameters

It is observed that the governing Eqs. (7–9) involve two non-dimensional material parameters, $E_f\left(\frac{1}{\mu_f}+\frac{1}{\mu_t}\right)$ and $E_t\left(\frac{1}{\mu_f}+\frac{1}{\mu_t}\right)$, which can be equivalently expressed in terms of elastic moduli ratio $E_t/E_f$ in the transverse and fiber directions, and $\sqrt{E_fE_t}\left(\frac{1}{\mu_f}+\frac{1}{\mu_t}\right)$ that represents the ratio of elastic to shear moduli.

### 3.2. Stress distribution

Prior to first microcrack nucleation, the normal stress in the first intact 90° ply ($n = N_{\text{crack}} + 2$) has a maximum at $x_2 = 0$ due to stress concentration induced by the pre-crack. Once the first microcrack is nucleated at $x_2 = 0$, the stress at $x_2 = 0$ becomes zero and the maximum stress in the ply occurs at a finite distance above (or below) the crack plane. Fig. 4 shows the stress distribution in the ply ($n = N_{\text{crack}} + 2$) for two non-dimensional material parameters $E_t/E_f = 0.16$ and $\sqrt{E_fE_t}\left(\frac{1}{\mu_f}+\frac{1}{\mu_t}\right) = 32.5$, pre-crack length $a = 4t$, and facesheet thickness $b = 20t$, where $\sigma$ is normalized by the applied stress $\sigma_{\text{applied}}$ and $x_2$ is normalized by the ply thickness $t$. A maximum value $\sigma_{\text{peek}}$ is clearly

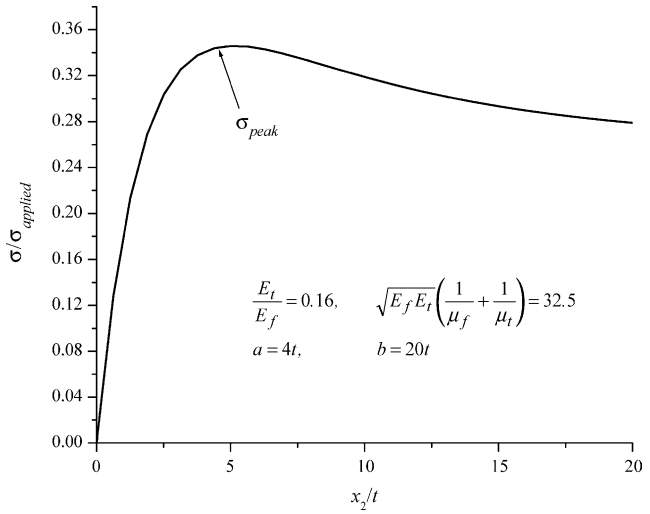


Fig. 4. Stress distribution (normalized by the applied stress $\sigma_{\text{applied}}$) in the 90° ply next to the pre-crack tip, in which the first microcrack is nucleated; It has a maximum stress $\sigma_{\text{peak}}$; $x_2$ is normalized by the ply thickness $t$, $a = 4t$ is the pre-crack length, $b = 20t$ is the facesheet thickness; $E_f$ and $E_t$ are the elastic moduli in the fiber and transverse directions, respectively, and $\mu_f$ and $\mu_t$ are the shear moduli.

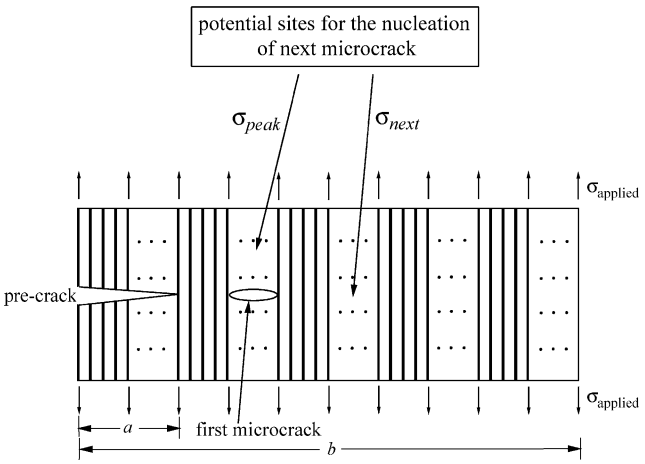


Fig. 5. A schematic diagram of the potential sites of microcrack nucleation after the first microcrack is nucleated in the 90° ply next to the pre-crack tip; $a$ is the pre-crack length and $b$ is the facesheet thickness; $\sigma_{\text{applied}}$ is the applied stress, $\sigma_{\text{peak}}$ is the peak stress in the 90° ply with the first microcrack, while $\sigma_{\text{next}}$ is the stress on the crack plane in the next 90° ply.

observed, where

$$\sigma_{\text{peak}} = \max_{0 \le x_2 < +\infty} \sigma_{N_{\text{crack}}+2}(x_2). \tag{15}$$

The location of peak stress is a potential site for the nucleation of next microcrack in this ply, as shown schematically in Fig. 5. From dimensional analysis, the peak stress depends on two non-dimensional material parameters $E_t/E_f$ and $\sqrt{E_fE_t}\left(\frac{1}{\mu_f}+\frac{1}{\mu_t}\right)$, and normalized pre-crack length $a/t$ and facesheet thickness $b/t$, i.e.

$$\sigma_{\text{peak}} = \sigma_{\text{applied}} \sum_{\text{peak}} \left[ \frac{E_t}{E_f}, \sqrt{E_fE_t}\left(\frac{1}{\mu_f}+\frac{1}{\mu_t}\right), \frac{a}{t}, \frac{b}{t} \right], \tag{16}$$

where $\Sigma_{\text{peak}}$ is a non-dimensional function determined from the shear-lag model.

### 3.3. Crack growth versus crack blocking

Another potential site for the next microcrack nucleation is on the crack plane ($x_2 = 0$) in the next intact 90° ply ($n = N_{\text{crack}} + 4$), which is to the right of first microcrack as shown schematically in Fig 5. The stress at this location is denoted by

$$\sigma_{\text{next}} = \sigma_{N_{\text{crack}}+4}(x_2 = 0), \tag{17}$$

which takes the form

$$\sigma_{\text{next}} = \sigma_{\text{applied}} \sum_{\text{next}} \left[ \frac{E_t}{E_f}, \sqrt{E_fE_t}\left(\frac{1}{\mu_f}+\frac{1}{\mu_t}\right), \frac{a}{t}, \frac{b}{t} \right], \tag{18}$$

where $\Sigma_{\text{next}}$ is a non-dimensional function determined from the shear-lag model.

For $\sigma_{\text{peak}} > \sigma_{\text{next}}$, the next microcrack will be nucleated at the location of $\sigma_{\text{peak}}$ (Fig. 5) at a finite distance above the first microcrack in the same 90° ply. On the contrary, the next microcrack will be nucleated on the crack plane in

the next 90° ply ($n = N_{\text{crack}} + 4$; Fig. 5) if $\sigma_{\text{peak}} < \sigma_{\text{next}}$. We use the ratio $\sigma_{\text{peak}}/\sigma_{\text{next}}$ as a simple indicator for the competition between the mechanisms of crack blocking (Fig. 2b) and crack growth (Fig. 2a), i.e.

$$\frac{\sigma_{\text{peak}}}{\sigma_{\text{next}}} > 1 \tag{19}$$

for crack blocking. The left hand side of the above equation depends on the length $a$ of the pre-crack, as seen from Eqs. (16) and (18). The numerical results have shown that, for all possible length of the pre-crack, $2t \le a \le b - 4t$, or equivalently $2 \le N_{\text{crack}} \le N_{\text{total}} - 4$, the left hand side of Eq. (19) always has a minimum value when $a = 2t$. Therefore, if we enforce that the minimum value of $\sigma_{\text{peak}}/\sigma_{\text{next}}$ at $a = 2t$ is larger than unity, the next microcrack will be nucleated in the same ply as the first microcrack regardless of the length of the pre-crack, i.e.

$$\left.\frac{\sigma_{\text{peak}}}{\sigma_{\text{next}}}\right|_{a=2t} > 1. \tag{20}$$

For given $E_t/E_f$ and $\sqrt{E_f E_t}\left(\frac{1}{\mu_f} + \frac{1}{\mu_t}\right)$, Eq. (20) gives a critical normalized facesheet thickness $b/t$ above which the crack blocking is ensured. This critical facesheet thickness, determined from $\left.\frac{\sigma_{\text{peak}}}{\sigma_{\text{next}}}\right|_{a=2t} = 1$, is independent of the pre-crack length. In other words, for each $\sqrt{E_f E_t}\left(\frac{1}{\mu_f} + \frac{1}{\mu_t}\right)$ and normalized facesheet thickness $b/t$, there exists a critical elastic moduli ratio $E_t/E_f$ below which the crack blocking is ensured. Surprisingly, the numerical results show that the critical elastic moduli ratio $E_t/E_f$ is independent of $\sqrt{E_f E_t}\left(\frac{1}{\mu_f} + \frac{1}{\mu_t}\right)$, and depends only on the ratio of the normalized facesheet thickness $b/t$. This can be seen in Fig. 6; for $b/t = 20$, the critical elastic moduli ratio $E_t/E_f$ is 0.105, and is independent of $\sqrt{E_f E_t}\left(\frac{1}{\mu_f} + \frac{1}{\mu_t}\right)$.

The relation between the normalized facesheet thickness $b/t$ and elastic moduli ratio $E_t/E_f$ which separates the crack

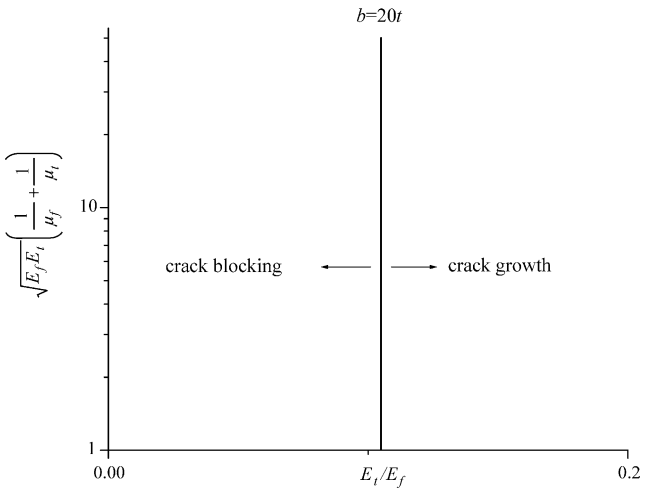


Fig. 6. For facesheet thickness $b = 20t$, the relation between $\sqrt{E_f E_t}\left(\frac{1}{\mu_f} + \frac{1}{\mu_t}\right)$ and $E_t/E_f$ which separates crack blocking from crack growth, where $t$ is the ply thickness, $E_f$ and $E_t$ are the elastic moduli in the fiber and transverse directions, respectively, and $\mu_f$ and $\mu_t$ are the shear moduli. This relation is found to be independent of $\sqrt{E_f E_t}\left(\frac{1}{\mu_f} + \frac{1}{\mu_t}\right)$.

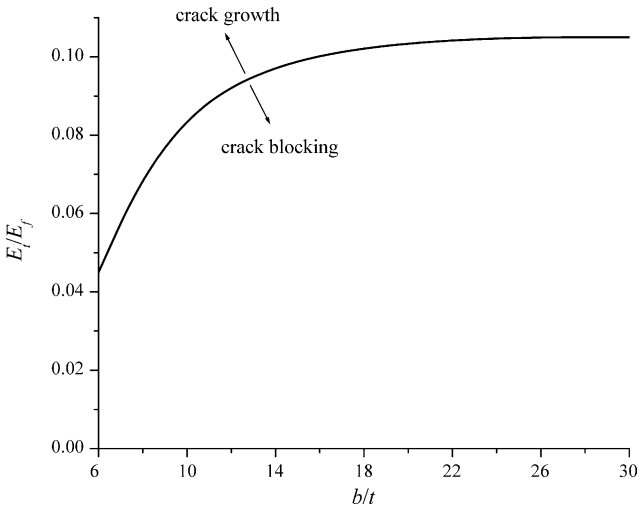


Fig. 7. The relation between normalized facesheet thickness $b/t$ and elastic moduli ratio $E_t/E_f$ that separates crack blocking from crack growth, where $t$ is the ply thickness, $E_f$ and $E_t$ are the elastic moduli in the fiber and transverse directions, respectively.

blocking from crack growth mechanisms is shown in Fig. 7. For a facesheet whose thickness $b$ (normalized by the ply thickness $t$) and elastic moduli ratio $E_t/E_f$ in the transverse and fiber directions below the curve in Fig. 7, the crack blocking is ensured and crack growth is prevented. For a thin facesheet $b/t = 6$ as in some aerospace applications, this requires the elastic modulus $E_t$ in the transverse direction must be less than 4.5% of the modulus $E_f$ in the fiber direction, or equivalently $E_f$ must be at least 23 times higher than $E_t$ to prevent crack growth. For a thicker facesheet $b/t = 30$ as in some naval applications, $E_t$ can be as large as 10% of $E_f$ such that the modulus in the fiber direction only needs to be 10 times higher the modulus in the transverse direction. The curve in Fig. 7 approaches a plateau for $b/t \ge 20$. Therefore, for thick facesheets as in some naval applications, the modulus ratio $E_f/E_t$ should be more than 10 in order to ensure crack blocking and prevent crack growth.

## 4. Concluding remarks

We have developed a shear-lag model to study two fracture mechanisms in facesheets of sandwich composites, namely crack growth and crack blocking. The shear-lag model gives a simple criterion governing these two mechanisms. For a given elastic moduli ratio $E_t/E_f$ in the transverse and fiber directions, there exists a critical facesheet thickness above which the crack blocking is ensured and crack growth is prevented. Equivalently, for a given facesheet thickness $b$, there exists a critical elastic moduli ratio $E_t/E_f$ below which the crack blocking is ensured. For $b = 6t$ ($t$ is the ply thickness), the elastic modulus $E_f$ in the fiber direction must be more than 23 times larger than the elastic modulus $E_t$ in the transverse direction

in order to ensure the crack blocking. For $b \geq 20t, E_f$ only needs to be 10 times larger than $E_t$.

## Acknowledgements

Y.H. acknowledges the support from ONR Composites for Marine Structures Program (grants # N00014-01-1-0205, Program Manager Dr Y. D. S. Rajapakse) and insightful discussions with C. T. Sun and V. Deshpande. C.L. was supported financially by the US Department of Energy, Defense Programs and the Laboratory Directed Research and Development (LDRD) program.

## References

[1] Hall DJ, Robson BL. A review of the design and materials evaluation program for the grp/foam sandwich composite hull of the ran minehunter. Composites 1984;15:266–76.
[2] Hall DJ. Examination of the effects of underwater blasts on sandwich composite structures. Compos Sturct 1989;11:101–20.
[3] Kuhn P. Stresses in aircraft and shell structures. New York: McGraw-Hill; 1956.
[4] Cao HC, Evans AG. On crack extension in ductile/brittle laminates. Acta Metall Mater 1991;39:2997–3005.
[5] Huang Y, Zhang HW, Wu F. Multiple cracking in metal-ceramic laminates. Int J Solids Struct 1994;31:2753–68.
[6] Budiansky B, Hutchinson JW, Evans AG. Matrix fracture in fiber reinforced ceramics. J Mech Phys Solids 1986;34:167–89.
[7] IMSL, IMSL(R) Fortran 90 MP library version 4.01, San Ramon: McGraw-Hill; 1999.